Predicting ash deposition behaviour for co-combustion of palm kernel with coal based on CFD modelling of particle impaction and sticking

Xin Yang [a], Derek Ingham [a], Lin Ma [a*], Alan Williams [b], Mohamed Pourkashanian [a]

[a] Energy Engineering Group, Energy-2050, Department of Mechanical Engineering, University of Sheffield, Sheffield S10 2TN, UK

[b] Energy Research Institute, School of Chemical and Process Engineering, University of Leeds, Leeds LS2 9JT, UK

[*]Corresponding author:

Email: lin.ma@sheffield.ac.uk Phone: +44 (0) 114 21 57212.

Abstract:

A CFD model that simulates particle impaction and sticking has been developed for predicting the ash deposition characteristics for the co-combustion of South African Coal (SAC) and palm kernel expeller (PKE) in an entrained flow reactor. The numerical related errors, caused by interception and the improper resolving of the flow-field within the boundary layer near the deposition surface, are investigated. In order to minimize the numerical related errors without excessive meshing, a new revised particle impaction model has been developed and accomplished using an impaction correction factor. The particle sticking is predicted based on the molten fraction results that have been obtained from the chemical equilibrium calculations using the chemical fractionation data in order to consider the short residence time of fly ash particles. The simulation results show that a reasonable coarse mesh, coupled with the revised particle impaction model, is suitable to accurately resolve the particle impaction without using a prohibitive meshing size. The ash deposition behaviour is determined by the particle impaction and sticking properties. Good agreements are obtained between the predicted results and the experimental data for the ash deposition behaviour.

Keywords: Ash deposition, CFD, revised particle impaction model, particle sticking, co-firing.

1 Introduction

Co-combustion of biomass with coal has been used as a near term measure to reduce CO_2 emission from coal fired power plants [1, 2]. Currently, co-firing 10-20% (thermal) biomass with coal has been widely used in power stations in the UK and Europe and a higher co-firing rate is also used. Further, some power stations, such as the Drax in the UK, are being converted to firing 100% biomass. With the recent announcement of the new EU targets of reducing gas emissions, fuel flexibility is likely to be one of the key factors influencing the operation of the power stations in the future, and the uses of various biomass and waste for power in the EU are expected to substantially increase. Currently most large scale power stations are using relatively clean biomass such as wood pellets, and to some extent straw, olive stones and palm kernel expeller (PKE). An addition of up to about 10-20% biomass has only moderate effects on the ash deposition in the furnace. However, with an increased co-firing rate and the use of a wide range of biomass sources, ash related problems are ranking high on the list of significant operational constraints in co-firing power plants [3, 4]. Ash deposition reduces the efficiency of the heat transfer through the water walls and heat exchangers and causes corrosion of boiler tubes, which may lead to reduced generating capacity and unscheduled outages [5]. Therefore, an improved understanding of the ash deposition in firing various types of biomass is imperative for an efficient boiler operation and optimization in the future [6].

The optimum biomass co-firing rate in coal-fired boilers has still been mainly determined by experiments up to now [4]. Computational Fluid Dynamics (CFD) has been widely used for solid fuel combustion simulations and various sub-models have been developed for predicting ash depositions in lab-scale test facilities as well as for full scale boilers [3-13]. Considerable progress has been made in the last decades in developing ash deposition models for CFD simulations [3-5, 14-17], and more detailed and accurate sub-models for combustion, fuel/ash particle transport, and sticking and deposition rate predictions have been developed [3, 16]. Typically, Lagrangian methods are employed to compute the trajectories of ash particles, coupled with an Eularian method for flow and gaseous phase reaction, where the inertial impaction of particles are often considered as the only or main mechanism for ash deposition formation. Therefore, accurate prediction of the particle impaction is a critical factor that affects the modelling of the ash deposition. The impaction efficiency of the particles is usually assumed to be unity which represents the worst scenario in terms of ash deposition rate [3, 16]. In practice the impaction efficiency can be much lower than this depending on the size, shape and density of the particles and the nature of the depositing surface. Weber et al. [17] investigated the requirements for accurate predictions of the impaction efficiency of fly ashes in a 2D geometry using the RANS- based CFD methods. It was concluded that only when the flow-field in the neighbourhood of the deposition surfaces is accurately resolved can accurate predictions of the particle impaction be obtainable by using the RANS- based CFD methods, especially for small particles since their trajectories are strongly affected by the boundary layer development. Haugen et al. [18, 19] applied direct numerical simulation (DNS) to investigate the particle impaction behaviour on cylinders and superheater tube bundles in a crossflow in order to accurately resolve the boundary layers around the cylinders. It should be noted that in these models [17-19], extremely fine grid for RANS or DNS is needed. However, this requirement is difficult to be satisfied in the simulation of an industrial boiler in order to predict ash deposition behaviours [17]. Often predicting major operational parameters such as the boiler temperatures and/or combustion properties may be achieved by using a reasonably coarse computer mesh. However, this reasonably coarse mesh can still lead to a significant error in ash particle impaction efficiency calculation [17].

In addition to the particle impaction, the stickiness of the ash particles plays a critical role in the formation of ash deposit and related slagging and fouling. The stickiness of an ash particle can be determined based on such as the viscosity, kinetic energy and degree of molten of fly ash particles. In terms of viscosity based sticking models, a reference viscosity is used to determine the stickiness. The value of the reference viscosity ranges within $8\text{-}10^8$ Pa.s which makes the sticking model strongly sensitive to the reference viscosity and may contribute to an inaccurate stickiness prediction [4, 20]. In addition, the kinetic energy thresholding sticking model, based on the Johnson-Kendall-Roberts (JKR) theory [14, 21, 22], has been proposed which takes into account the kinetic energy of the particles and the surface energy of both the particle and the impacted surface. However, a fitting process was necessary to develop the effective Young's modulus versus the particle temperature and the particle diameter by matching the experimental data with the simulation results [14]. Further, the molten fraction-based sticking model has been developed using slag calculations based on the chemical equilibrium of the ash composition and it was found that deposition models based on the molten fraction of ash particles calculated from chemical equilibrium are promising [20].

Therefore, this paper aims to develop an improved ash deposition CFD model through (i) a new revised particle impaction model to minimize the numerical related errors with an affordable number of computational mesh, and (ii) an appropriate particle sticking model based on the ash chemistry and the particle momentum for the PKE where there is relatively a scarce amount of data available. The model developed has been tested using the experimental data from Imperial College's entrained flow reactor [23, 24], where PKE with the high level of phosphorus has been considered.

2 Source of experimental data

Figure 1 shows a schematic geometry of the entrained flow reactor (EFR) located at Imperial College London. It consists of four electrically heated furnaces with a diameter of 0.1 m and a length of about 5 m. The burner consists of a primary inlet through which the pulverized coal and the primary air are fed, and a secondary inlet for the heated air. The uncooled ceramic probe is placed at the sample port 2 to collect the ash deposits, which has a furnace temperature of approximately 1250 ^{o}C. More details of reactor can be found in [23, 24].

EFR has been used in coal/biomass studies for many years and this is because it can provide information on volatile release, char combustion, as well as ash deposition of the fuel combustion processes in an environment that is close to that observed in an industrial furnace [23]. The time-temperature history of fuel particles in the EFR is one of the key parameters for the design and operation of EFR tests to achieve a similar condition as in a power plant in the study of ash deposition. This has been carefully designed and operated in the experiments where a fuel particle with the residence time of approximately 3 seconds has been achieved [23]. The probe that is used for collecting deposits is placed in the cross section of the EFR to simulate the deposition formation on the heat exchanger which are governed mainly by the cross-flow flue gas streams [17, 23]. Figure 2 shows a schematic diagram of the typical structure of the deposition layers formed on the front surface of a heat exchanger tube. The initial layer is typically formed due to the thermophoresis of small particles and the condensation of alkali vapour compounds, such as NaCl, KCl, Na_2SO_4, and K_2SO_4 [25-33]. This initial layer is usually porous and has a low thermal conductivity. The lower surface temperature of the tube enhances the growth of the initial layer and as a result the surface temperature of the deposit will increase to a point that can facilitate the melt and sintering to form a slag/sintered layer. The further growth of the slag/sintered layer is then dictated by the inertial impaction of larger fly ash particles. The slag/sintered layer will has a higher thermal conductivity compared to the initial layer because of its dense structure and the more melt formed at the layer, and the grain size is also larger than that formed at the initial layer [26-29].

A range of scenarios of co-firing coal and biomass fuels have been experimentally investigated with the Imperial College EFR, where ash depositions were collected and subsequently analysed. The experimental data for the co-combustion of palm kernel expeller (PKE) with South African coal (SAC) has been employed in this paper. The fuel properties, including proximate and ultimate analysis, as well as ash compositions, of both coal and PKE are summarized in Table 1 [24, 34, 35]. As expected, PKE has much lower values of fixed carbon and ash contents than the SAC but a higher volatile content. With regard to the ash composition, SAC is mainly composed of acid oxides (silicon and aluminium) whereas PKE is mainly composed of phosphorus, potassium and alkaline earth metals. Biomass with an ash rich in alkali metals and chlorine have shown a tendency to accelerate the process of deposition, slagging and fouling on the boiler surfaces [30-32]. The situation for phosphorus-rich biomass fuels is more complex and relatively few research works and data are available. In very general terms, high potassium and high phosphorus ashes tend to have a low fusion temperature and thus show a higher slagging tendency. However, depending on the overall compositions of the fuel and ash, phosphorus can combine with the reactive alkali/alkaline species, e.g. potassium, calcium and magnesium, to form higher melting temperature phases [36, 37], and it can also influence the release of potassium during combustion, thus it can reduce the overall ash depositions tendency [36, 37]. In the experiments preformed at the EFR, an uncooled ceramic probe is employed and placed at the sample port 2 (which has a furnace temperature of approximately 1250 ^oC) to collect the ash deposits, representing a slag/sintered layer [23, 24, 38]. Therefore, in the current study, the initial layer is not modelled and the inertial impaction of particles is considered as the main factor in controlling the ash deposition on the tube [8].

3 Mathematical models

3.1 Combustion models

In this paper, the combustion of coal and biomass is modelled in a combined Eularian-Lagrangian frame of reference where the volatile combustion is modelled in the Eularian frame of reference and the fuel/ash particles are tracked in a Lagrangian frame of reference. As stated in our previous papers, the single kinetic rate model was employed for the devolatilizations of the coal and biomass, where the rate of devolatilization depends on both the temperature and the volatile content of the particles [1, 39]. We have used the values of the Arrhenius rate constants, pre-exponential factor and activation energy that have been previously used and validated [1, 39, 40]. The combustion of the volatile gases was modelled using the Eddy Dissipation Model with a two-step global reaction mechanism [41]. Also it is assumed that the particle size remains constant, while the particle density reduces during the release of the volatile gases from the fuel particles [4, 39].

Char combustion was modelled with the intrinsic char combustion model, which assumes that the order of the surface reaction is unity and that the surface reaction rate includes the effects of both the bulk diffusion and chemical reaction rates [1]. The same model constants were employed as [41-43]. In the Smith intrinsic model, the variation of the char particle size and density is related to the fractional degree of burnout, U, in terms of the burning mode, α, as follows [7, 42]:

$$\left(d_p/d_{p,0}\right) = (1-U)^{\alpha} \tag{1}$$

$$U = [1-(m_p/m_{p,0})] \tag{2}$$

where d_p and m_p are the char particle size and mass, respectively, and the subscript zero refers to the initial conditions (at the start of the char combustion). For the coal, the value of α used was 0.25, and this corresponds to a decrease in both the particle size and density during combustion [7, 42]; for the biomass, it is believed that the particles would most likely maintain their original size during combustion, and therefore the value of zero was used for α, and this corresponds to a constant size but with a decreasing density of the particle during combustion [40].

The trajectories of the coal and biomass particles are governed by the particle momentum equation, which is a balance of the drag, gravity, and other body forces as formulated in the following equation [7, 44]:

$$\frac{d\vec{v}_p}{dt} = \frac{18\mu_g}{\rho_p d_p^2}\frac{C_D Re_p}{24}\left(\vec{v}_g - \vec{v}_p\right) + \frac{\vec{g}(\rho_p - \rho_g)}{\rho_p} + \vec{F} \tag{3}$$

where $\vec{v}$, ρ, μ and d are the velocity, density, viscosity and diameter of the particles, respectively; the subscripts p and g refer to the particle and gas, respectively, C_D is the drag coefficient, and $\vec{F}$ is other body forces, such as the thermophoretic force, virtual mass force, etc. The thermophoretic force, which is caused by the temperature gradient in the gas stream close to a solid depositing surface may be neglected when modelling a heavily deposited surface such as the slag/sintered tube surface where a high surface temperature exists. The virtual mass force, which is due to the acceleration of the fluid around the particle, may also be ignored when the density of the particle is much greater than the density of the fluid.

In order to better resolve the particle trajectories in the boundary layer, the gas flow boundary layer has to be modelled carefully [17] and the enhanced wall treatment was used. If the near-wall mesh is fine enough to be able to resolve the fluid viscous sublayer, then the enhanced wall treatment will be identical to the traditional two-layer zonal model [45]. If a coarse mesh is used together with a wall-function, the accuracy of the near wall modelling will not significantly be reduced when the enhanced wall treatment is used, where a single wall law for the entire wall region is generated by blending the linear (laminar) and the logarithmic laws of the wall [46].

The energy balance equation of the particles, which are solved along the trajectories of the particles in order to obtain the corresponding particle temperatures, is given as follows [1, 7, 11]:

$$m_p c_p \frac{dT_p}{dt} = hA_p\left(T_\infty - T_p\right) + \varepsilon_p A_p \sigma\left(\theta_R^4 - T_p^4\right) - Q_p \tag{4}$$

where m_p, c_p, T_p, A_p, and ε_p are the mass, specific heat, temperature, surface area and emissivity of the particles, T_∞ is the gas temperature, σ is the Stefan–Boltzmann constant, and θ_R is the radiation temperature. Q_p, which is the latent heat or the heat of reaction is determined by the following equations:

$$Q_p = \begin{cases} 0, & \text{if under the step of inert heating or cooling} \\ \dfrac{dm_p}{dt} h_{fg}, & \text{if under the step of devolatilization} \\ f \dfrac{dm_p}{dt} H_r, & \text{if under the step of char combustion} \end{cases} \tag{5}$$

where h_{fg} is the latent heat, f is the fraction of the heat absorbed by the particles, and H_r is the heat of reaction released by the surface reaction. The radiative heat transfer was modelled using the Discrete Ordinates model and the gas absorption coefficient was calculated with the domain based Weighted Sum of Gray Gases Model (WSGGM).

3.2 Revised particle impaction model

Due to the influence of the gas flow, not all the particles carried by the gas stream will impact on the depositing surface. The amount of ash particles that may hit a depositing surface can be estimated by the particle impaction efficiency, which is defined as the percentage of particles of given size in the projected area of deposition surface in the upstream gas flow that can impact on the deposition surface [17]. The impaction efficiency is dependent on the particle Stokes number [47, 48] that is defined as follows for particle impaction on a circular cylinder:

$$\mathrm{St} = (\rho_p d_p^2 u_p)/(9\mu_g D) \quad (6)$$

where ρ_p, d_p, u_p, and μ_g are the particle density, particle diameter, bulk particle velocity and gas dynamic viscosity, respectively, and D is the outer diameter of the deposition pipe. Particles with larger Stokes number are less likely to be affected by the gas flow and more likely to impact on the surface of the deposition pipe; however, particles with smaller Stokes number follow more closely to the fluid streamlines and are less likely to impact on the surface [48]. Therefore, accurately predicting the gas flow in the boundary layer near the deposition surface is very important for accurate predicting the particle impaction efficiency, in particular for particles with a small Stokes number. However, this often requires an extremely fine computer mesh close to the deposition surface in order to resolve the flow boundary layer accurately and this is often prohibitively expensive computationally for modelling real combustors and industrial boilers. In most cases, as seen in most publications, a reasonably coarse mesh is employed to satisfy the mesh independency requirement for the bulk of the gas flow. However, with this reasonably coarse mesh the particle impacting efficiency is often over-estimated [12, 17], since the trajectory of small ash particles close to a deposition surface is very sensitive to details of the boundary layer flow, leading to errors in the deposition rate prediction.

Further, during the particle tracking in CFD, the particle is usually treated as a point in the computational domain and whether a particle hits a wall or not is determined by the position of the center of the particle without considering the effect of the size of the particle [17, 18]. However, in reality, a particle will hit the surface with a distance equal to the particle radius away from the centre of the particle [17, 18]. This interception effect of the particle size on the impaction efficiency can be described using the interception parameter, R, defined as follows [17, 18]:

$$R = d_p/D \quad (7)$$

where d_p and D are referred to the diameters of the particles and the deposition probe. Clearly the larger the ratio of particle diameter and the tube diameter, the larger is the interception. In order to remove the errors resulting from using a coarse computational mesh in the boundary layer and from the particle interceptions, an impaction correction factor, F, may be introduced which can be defined as the ratio of the real particle impaction efficiency and that predicted using a reasonably coarse computational mesh for a particular particle stream, i.e. for the ith particle stream, $F_i = I_{real,i}/I_{coarse,i}$. The real impaction efficiency $I_{real,i}$ can be estimated by using a small computational domain that only contains part of the furnace that is close to the superheat tubes where extremely fine meshing may be used. The boundary conditions for flue gas and ash particle flows may be taken from the existing results obtained using the reasonably coarse computational mesh. If the interception parameter is also considered then the impaction correction factor may be calculated using the following equation:

$$F_i = (I_{fine,i} + R_i)/I_{coarse,i} \quad (8)$$

where $I_{fine,i}$ is the predicted particle impaction efficiency from a well resolved boundary layer, $I_{coarse,i}$ is the impaction efficiency from a reasonably coarse mesh, and R_i is the interception parameter, of the i th particle stream; This impaction correction factor can be used to correct the CFD predicted mass flux, i.e. the arrival rate of the particles to the deposition surface still using a reasonably coarse computational mesh in the CFD simulation as illustrated in Figure 3.

In order to validate the proposed approach for improving the accuracy of particle impaction efficiency calculations, particle impactions on a two-dimensional cylinder have been simulated and compared with the results from the direct numerical simulation (DNS) reported by Haugen and Kragset [18]. Figure 4 shows the flow configuration and boundary conditions employed. A computational domain of 6D×12D is employed with the tube being placed in the centre of the domain. The diameter of the tube D=40mm. Gas (viscosity=4.6×10^{-5} Pa.s and density=0.245 kg/m^3, which represent a stream of hot flue gas under 1500 K [17]) enters into the domain with a given free stream velocity, U_0. Two velocities, U_0= 0.47 m/s and 7.91 m/s have been considered, which corresponding to a Reynolds number (Re_t, based on deposition tube diameter) approximately 100 and 1685, respectively. In order to obtain the impaction efficiency with a well resolved boundary layer mesh, i.e. I_{fine}, RANS simulation with a fine mesh of approximately 400 nodes ($Re_t = 100$) and 1600 nodes ($Re_t = 1685$) on the tube circumference have been employed as suggested by [17, 18, 49]. Figure 5 compares the predicted particle impaction efficiencies with and without the corrections for the two cases investigated with the DNS results obtained from [18]. Reasonably coarse meshes with approximately 140 nodes and 180 nodes on the circumference of the tube for the $Re_t = 100$ and Re_t = 1685 cases respectively have been employed. It shows that the impaction correction factor increase with larger particle Stokes number and the value of the correction factor is approaching one when the Stokes number is greater than 1. Also, it can be found that applying the revised particle impaction model can substantially to decrease the errors in the predicted particle impaction efficiency when a coarse mesh is used, compared with the results from the DNS.

3.3 Particle sticking model

After particles reach a deposition surface, not all the arriving particles will stick to the surface. If the particle, or the deposition surface, is sticky then the particle may deposit [10]. On the other hand, particles with high impact energy may rebound back into the gas flow after hitting the wall [13, 15]. The sticking efficiency of the impacting particles is defined as the ratio of the number of particulates depositing on the surfaces to the number of the particles impacting on the surfaces [6]. There are at least two factors influencing the particle sticking efficiency, namely, (i) whether a particle is sticking or not and (ii) whether the particle will rebound back from the surface. In this work, the stickiness of the particles was determined by the degree of melting of the particle, i.e. the molten fraction of the particles [20] calculated based on the thermodynamic equilibrium of the particles. Since not all ash components can reach chemical equilibrium when arriving at the deposition surface, in particular for EFR test conditions [50], the chemical fractionation analysis data is employed from a stepwise leaching of the relevant fuels in order to consider the short residence time of the ash particles in the reactor [50]. The chemical thermodynamics software package FactSage 6.4. is employed to perform the thermodynamic equilibrium calculations based on the minimization of the Gibbs free energy from the system subject to the mass balance constraints [51, 52].

In the thermodynamic equilibrium calculations, the gas composition N_2, O_2, CO_2 and H_2O are taken from the CFD predictions and their amounts are dictated by the inlet air/fuel ratio. The reactants in the ash are obtained from the ash analysis shown in Table 1 and the chemical fractionation data from [53, 54] for both SAC and PKE as shown in Table 2. Potassium and sodium can be completely leached with chemicals such as water and acetate for PKE whereas only part of sodium can be leached for SAC. Phosphorus is more difficult to be leached for both PKE and SAC. The amount of the non-reactive fraction of the inorganic mater in the ash particles which can reach equilibrium during combustion is difficult to determine through the experiments and this amount is typically in the range 0 to 25% depending on particle size, temperature and residence time, etc. [15, 50, 53, 55, 56]. Hence, in this paper, a middle value of 10% was chosen [50]. For particles impacting a slagging/sintered surface, the value for the non-reactive fraction is less significant in predicting the overall sticking efficiency than impacting on a new tube surface.

The calculations were performed for a temperature range between 1500 K and 1750 K at a temperature interval of 20 K and at atmospheric pressure. The possible products selected are the entire compound species (ideal gases and pure solids) from the ELEM, FToxid, FTsalt and FACTPS databases. The slag model chosen in the calculations was the 'SLAGC' with possible 2-phase immiscibility to consider the relative high amount of phosphorus in the ash [57, 58], which covers oxide liquid solutions of MgO, FeO, Na_2O, SiO_2, TiO_2, Ti_2O_3, CaO, Al_2O_3 and phosphates as $Na_3(PO_4)$, $Ca_3(PO_4)_2$, $Mg_3(PO_4)_2$ and $Fe_3(PO_4)_2$, K_3PO_4 and $FePO_4$.

As mentioned earlier, whether an impacting particle actually sticks or not depends on whether the particle rebounds from the deposition surface or not, and this depends on the deformation after particle impacts on the surface and the momentum of the particles [8]. The particle energy balance model, developed by Mueller et al. [15] and Mao et al. [59], was employed to assess the excess energy , E_x, which is the excess rebounding energy particles possess after impaction and can be calculated using the following empirical formula [13, 15, 59]:

$$E_x = \frac{D^2}{4}(1 - cos\alpha) - \frac{3D^{2.3}}{25}(1 - cos\alpha)^{0.63} + \frac{2}{3D} - 1 \quad (9)$$

where D is the ratio of the maximum deformation in the particle diameter to the actual particle diameter, and α is the static contact angle of the particle. D is related to the particle Weber number, We, and the Reynolds number, Re, as follows:

$$D = (12 + We)^{0.5} \cdot [3(1 - cos\alpha) + 4(We/Re^{0.5})]^{0.5} \quad (10)$$

$$We = (\rho_p U_n^2 d)/\sigma \quad (11)$$

$$Re = (\rho_p U_n d)/\mu_p \quad (12)$$

where U_n is the impact velocity component normal to the impact surface, and σ is the particle surface tension. If a particle possesses the necessary excess energy, $E_x > 0$, the particle will bounce off the surface, otherwise it will stick.

4 EFR CFD model set up and results

4.1 Model set up

In this paper, co-firing PKE with South Africa coal with four different co-firing rates have been investigated, namely the SAC are blended with 0, 20, 40 and 60 wt.% of the PKE. The same EFR operational conditions as indicated in Figure 1 were employed for all four cases investigated. The coal flow rate of 0.014 gs^{-1}, the primary air flow rate of 0.067 kgs^{-1} at 70 ^{o}C, and the secondary air flow of 1.167 kgs^{-1} at 300 ^{o}C [8] have been used for all the cases. Only the biomass additions were different to make PKE 0, 20, 40 and 60 wt.% of the fuel flow rate. Typically EFR was operated at a relatively low Reynolds number of approximately 400, to acquire near laminar flow conditions in the reactor although low turbulence occurs near the burner region [23]. To improve the convergence of the CFD model, the Transition SST turbulence model which is applicable to low Reynolds number flows, was chosen to simulate the gas flow [60, 61]. The particle size of the SAC used ranged between 1 µm and 95 µm with a mean diameter of 50 µm and the particle size of the PKE ranged between 105 µm and 355 µm, with a mean diameter of 130 µm [16, 17, 20]. The temperature of the internal wall of the EFR has been specified according to the experimental conditions as indicated in Figure 1. The adiabatic condition has been employed at the surface of the deposition probe to consider its uncooled condition. The commercially available CFD software package ANSYS Fluent version 15.0 has been employed to perform the basic calculations of the coal and biomass combustion incorporating the in-house developed User Defined Functions and Memories in order to model the ash deposition process with the revised particle impaction model and the particle sticking model.

Six different meshes consisting of 0.5, 0.7, 1.1, 1.6, 2.0, and 3.3 million hexahedral cells have been employed to investigate the effect of mesh on the CFD solutions. The mesh is refined in the vicinity of the probe and the injection region, as well as in the burner region. Both the typical gas flow properties, such as the distributions of the gas temperature and gas velocity and the arrival rate of fly ash particles that impact the probe surface were examined. It was found that independent solutions for the gas temperature and velocity in the bulk of the EFR may be obtained using a mesh with no less than 0.7M cells which may be regarded as a reasonable coarse mesh. However, mesh independency was not achieved for the predicted arrival rate of fly ash particles until a mesh with a cell number of over 1.6M was used, as shown in Figure 6. It can be seen from Figure 6, if the 0.7M cell mesh is employed, then the arrival rate of the impacting particles would be overestimated by approximately 40% compared to the results obtained using 1.6M cells. This is because a higher impaction efficiency is predicted for all the particles as shown in Figure 6. It should be noted that for industrial boilers, the gas flow is highly turbulent ($Re \geq 100000$) and a very thin flow boundary layer will be formed, thus achieving a grid independent solution for particle impaction is usually very difficult in a 3D geometry [17].

In this particular case of the Imperial EFR, the particle impaction results obtained from, using the 1.6M grid was taken as I_{fine} since they are mesh independent solutions for the particle impaction, and the particle impaction results from the 0.7M grid was taken as I_{coarse} since they are mesh independent solutions of the gas flows. For the case investigated, the interception parameter, R, is in the range 2.9×10^{-5} to 7.5×10^{-3} which give an overall effect on the particle collection efficiency in the range of 7-8% and therefore cannot be ignored.

4.2 Predicted impaction efficiency and sticking efficiency

The modelling of the particle impaction and sticking is critical for predicting ash deposition formation and growth. As discussed in Section 3.2, both the improper resolving of the gas flow within the boundary layer near the deposition surface and particle interception can affect the accuracy of the predicted particle impaction in CFD modelling. Figure 7 shows the calculated impaction correction factor F_i and particle impaction efficiency as a function of the Stokes numbers of the coal and biomass particles employed in the EFR simulation for the four co-firing cases investigated. It can be found that the correction factor increases with an increase in the particle Stokes number. The value is approaching one when the Stokes number is greater than one because the particles are mainly driven by their inertia and the imperfection in the prediction of the boundary flow field is of secondary importance [17, 18]. However, particles with small Stokes number have a small value of the correction factor and this indicates that the numerical related errors are large when a coarse mesh was used and this is because the particle trajectories are strongly affected by flow field within the boundary layer which needs to be accurately modelled [17-19]. The predicted impaction efficiencies for particles with a similar Stokes number are similar for different levels of the PKE addition, in particular for low co-firing rates. This is because the air and fuel flow rates are almost the same for the four cases and this results in a similar flow distribution, including in the boundary layer flow.

Further, the figure shows that the Stokes number of most of the fuel particles is less than 1 and the maximum Stokes number is approximately 1.5, and this indicates the significance of the impaction correction factor in predicting the ash deposition rate. Figure 8 compares the results of the predicted overall impaction efficiencies both with and without applying the particle impaction correction. It can be observed that for all the cases, there is 30-50% over prediction in the overall impaction efficiency and this may be resulted if a coarse mesh is employed and no correction is made. Also the figure shows that on increasing the co-firing rates from 0-60%, the overall impaction efficiency increases from about 3.1% to 4.6%. This is due to the fact that the biomass particles have a higher value for the Stokes number than that of the coal particles due to the much larger particle size, and this results in a higher impaction efficiency than that of the SAC particles.

Figure 9 shows the predicted overall sticking efficiency (defined as the ratio of the overall mass flow rate of the deposited particles to the overall mass flow rate of the impacting particles) taking into consideration both the stickiness of the ash particles and the deposition surface for the four cases investigated. The figure shows that the overall sticking efficiency for the 60% PKE co-firing ratio is approximately 33%, which is the lowest of the four cases investigated. The overall sticking efficiencies are similar for the 20% and 40% ratio cases which lie in the range from 53% to 56%. This is because the molten fraction increases on adding 20% and 40% PKE co-firing ratio due to the larger amount of molten phases formed than in the case of 0% PKE co-firing ratio and then the sticking efficiency increases. However, the sticking efficiency decreases on adding 60% PKE. This is due to the formation of high temperature solid phases (such as $Ca_3(PO_4)_2$, $Mg_3P_2O_8$, $AlPO_4$, and $KAlSi_2O_6$) with increasing the alkaline earth metals (calcium and magnesium) by further adding the PKE.

It was noted that the sticking efficiencies for particles were almost the same for all Stokes numbers, with only a slightly increase with an increase in the Stokes number. This is because the particles were at the cooling stage at the end of the char combustion, the small particles cool earlier and more quickly and thus have a lower temperature and are less sticky than those of the larger particles [14].

4.3 Predicted ash deposition

In the experiments reported in [23, 24], the deposition efficiency, which was calculated for each EFR run based on the mass percentage of the fuel ash that impacts on the projected surface area of the probe that was retained in the collected deposit, was employed to evaluate the deposition propensity. Figure 10 shows a quantitative comparison between the computed deposits (with and without the revised particle impaction model) and the experimental data in terms of the deposition efficiency. In general, the predicted deposition efficiency without the revised particle impaction model is much higher than both the experimental data and the results obtained with the revised particle impaction model. The predicted deposition efficiency with the revised particle impaction model varies between 6.1% to 9.5% for the four cases investigated, which is in good agreement with the experimental data. Also the calculation results show that the deposition efficiency at the 60% PKE co-firing ratio is lower than that at 40% PKE co-firing ratio and the deposition efficiency is the highest for a co-firing ratio of 40% of PKE. The reason for this modelling outcome is due to the decreasing trend of the overall sticking efficiency at 60% PKE co-firing ratio. However, in the experimental data, the deposition efficiency with a value of 8.5% at 60% PKE co-firing ratio is still slightly higher than that at 40% PKE co-firing ratio which is 8.4%. The repeatability error for the measurement of the deposition efficiency can be up to 4.7% [24]. Therefore, the small disagreement in predicted the deposition efficiency between is acceptable [24, 62]. No obvious increase of deposition efficiency for co-combustion of PKE with South African Coal was found comparing with pure coal comustion both in the experimental results and the simulation results which is controlled by both the particle impaction and sticking, although higher sintering degree of the deposits was shown in the experiments. This is because the viscosity of the deposit was decreased with the decrease in SiO_2 and increase in MgO, CaO and P_2O_5 in the ash composition by adding PKE [24].

Comment [a1]: ??

5 Conclusions

An ash deposition model based on modelling the particle impaction and sticking has been developed for the modelling of ash deposition for co-combustion of coal and palm kernel. A revised particle impaction modelling approach is proposed in order to minimize the numerical related errors and avoid using an excessive mesh size. A particle impaction correction factor that takes account of both the effect of particle interception and errors in the particle impaction prediction when a coarse computational mesh is employed. The particle sticking is predicted based on the molten fraction of the particle obtained from the chemical equilibrium calculation using the chemical fractionation data of fuels in order to consider the short residence time of the fly ash particles.

The deposition efficiencies of co-firing SAC with PKE of four different ratios in the EFR have been calculated using the model and the results obtained have been compared with the experimental data obtained in the EFR. Reasonably good agreement was obtained and it demonstrated that the proposed model can reduce the numerical related errors in the ash deposition prediction using a reasonable coarse computational mesh adaqit for the combustion process simulation. The results suggested that the overall impaction efficiency of the particles increase with the increase in the co-firing ratio of PKE, whilst the overall stickiness efficiency may depend on the relative amount of high- and low- melting point compounds that are formed and this is dictated by the ash composition of the fuels.

It is noted that the Stokes numbers of most of the ash particles are less than one and thus a significance correction to the predicted ash deposition rate may be required and this depends on the number of computational meshes employed. When the particle Stokes number approaches or is greater than one then the particles are mainly driven by their inertia and the impact correction factor approaches one and therefore using a relatively coarse mesh may be acceptable.

Acknowledgment

The authors wish to thank Prof. J. Williamson (Imperial College, London) for the helpful discussions on the deposition behaviours in the co-firing experiments, Prof. R. Weber and Dr A.M. Beckmann (Clausthal University of Technology) for their very helpful advice on modelling particle impaction. Also X. Yang would like to acknowledge the China Scholarship Council and the University of Sheffield and University of Leeds, for funding his research studies. Support from the RCUK is also acknowledged.

References

[1] Black S, Szuhánszki J, Pranzitelli A, Ma L, Stanger PJ, Ingham DB, et al. Effects of firing coal and biomass under oxy-fuel conditions in a power plant boiler using CFD modelling. Fuel 2013;113:780-6.

[2] Rubiera F, Pis J, Pevida C. Raw materials, selection, preparation and characterization. In: Puigjaner L, editors. Syngas from Waste, London; Springer Verlag; 2011, p. 11-22.

[3] Lundmark D, Mueller C, Backman R, Zevenhoven M, Skrifvars BJ, Hupa M. CFD based ash deposition prediction in a BFBC firing mixtures of peat and forest residue. J Energ Resour-ASME 2010;132:031003/1-/8.

[4] Taha TJ, Stam AF, Stam K, Brem G. CFD modeling of ash deposition for co-combustion of MBM with coal in a tangentially fired utility boiler. Fuel Process Technol 2013;114:126-34.

[5] Wang H, Harb JN. Modeling of ash deposition in large-scale combustion facilities burning pulverized coal. Prog Energ Combust 1997;23:267-82.

[6] Akbar S. Numerical simulation of deposit formation in coal-fired utility boilers with biomass co-combustion [dissertation]. University of Stuttgart; 2011.

[7] Degereji MU, Ingham DB, Ma L, Pourkashanian M, Williams A. Prediction of ash slagging propensity in a pulverized coal combustion furnace. Fuel 2012;101:171-8.

[8] Garba MU, Ingham DB, Ma L, Degereji MU, Pourkashanian M, Williams A. Modelling of deposit formation and sintering for the co-combustion of coal with biomass. Fuel 2013;113:863-72.

[9] Huang LY, Norman JS, Pourkashanian M, Williams A. Prediction of ash deposition on superheater tubes from pulverized coal combustion. Fuel 1996;75:271-9.

[10] Kær SK, Rosendahl LA, Baxter LL. Extending the capability of CFD codes to assess ash related problems in biomass fired boilers. Prepr Pap - Am Chem Soc, Div Fuel Chem 2003;49:97-108.

[11] Lee FCC, Lockwood FC. Modelling ash deposition in pulverized coal-fired applications. Prog Energ Combust 1999;25:117-32.

[12] Losurdo M, Spliethoff H, Kiel J. Ash deposition modeling using a visco-elastic approach. Fuel 2012;102:145-55.
[13] Ma L, Pourkashanian M, Williams A, Jones J. A numerical model for predicting biomass particle depositions in a pf furnace. In: Proc ASME Turbo Expo 2006, Barcelona, Spain; 2006, p. 333-42.
[14] Ai W, Kuhlman JM. Simulation of coal ash particle deposition experiments. Energy Fuels 2011;25:708-18.
[15] Mueller C, Selenius M, Theis M, Skrifvars B-J, Backman R, Hupa M, et al. Deposition behaviour of molten alkali-rich fly ashes—development of a submodel for CFD applications. Proc Combust Inst 2005;30:2991-8.
[16] Mueller C, Skrifvars B-J, Backman R, Hupa M. Ash deposition prediction in biomass fired fluidised bed boilers - combination of CFD and advanced fuel analysis. Prog Comput Fluid Dyn 2003;3:112-20.
[17] Weber R, Schaffel-Mancini N, Mancini M, Kupka T. Fly ash deposition modelling: Requirements for accurate predictions of particle impaction on tubes using RANS-based computational fluid dynamics. Fuel 2013;108:586-96.
[18] Haugen NEL, Kragset S. Particle impaction on a cylinder in a crossflow as function of Stokes and Reynolds numbers. J Fluid Mech 2010;661:239-61.
[19] Haugen NEL, Kragset S, Bugge M, Warnecke R, Weghaus M. MSWI super heater tube bundle: Particle impaction efficiency and size distribution. Fuel Process Technol 2013;106:416-22.
[20] Wieland C, Kreutzkam B, Balan G, Spliethoff H. Evaluation, comparison and validation of deposition criteria for numerical simulation of slagging. Appl Energ 2012;93:184-92.
[21] Brach RM, Dunn PF. A mathematical model of the impact and adhesion of microsphers. Aerosol Sci Tech 1992;16:51-64.
[22] Johnson KL, Kendall K, Roberts AD. Surface energy and the contact of elastic solids. Proc R Soc London A: Math Phys Sci 1971;324:301-13.
[23] Hutchings IS, West SS, Williamson J. An assessment of coal-ash slagging propensity using an entrained flow reactor. In: Baxter L, DeSollar R, editors. Proceeding of a conference on Applications of Advanced Technology to Ash-Related Problems in Boiler. Proceedings of the Engineering Foundation Conference. Waterville Valley, New Hampshire. Plenum Press New York; 1995 vol. 1621. p. 201–22.
[24] Wigley F, Williamson J, Malmgren A, Riley G. Ash deposition at higher levels of coal replacement by biomass. Fuel Process Technol 2007;88:1148-54.
[25] Zhan Z, Bool LE, Fry A, Fan W, Xu M, Yu D, et al. Novel temperature-controlled ash deposition probe system and its application to oxy-coal combustion with 50% inlet O_2. Energy Fuels 2013;28:146-54.
[26] Zhou H, Zhou B, Dong K, Ding J, Cen K. Research on the slagging characteristics of easy to slagging coal in a pilot scale furnace. Fuel 2013;109:608-15.
[27] Zhou H, Zhou B, Li L, Zhang H. Experimental measurement of the effective thermal conductivity of ash deposit for high sodium coal (Zhun Dong coal) in a 300 kw test furnace. Energy Fuels 2013;27:7008-22.
[28] Zhou H, Zhou B, Li L, Zhang H. Investigation of the influence of the furnace temperature on slagging deposit characteristics using a digital image technique. Energy Fuels 2014;28:5756-65.
[29] Zhou H, Zhou B, Zhang H, Li L, Cen K. Investigation of slagging characteristics in a 300 kw test furnace: Effect of deposition surface temperature. Ind Eng Chem Res 2014;53:7233-46.
[30] Wang X, Xu Z, Wei B, Zhang L, Tan H, Yang T, et al. The ash deposition mechanism in boilers burning Zhundong coal with high contents of sodium and calcium: A study from ash evaporating to condensing. Appl Therm Eng 2015;80:150-9.
[31] Niu Y, Zhu Y, Tan H, Hui S, Jing Z, Xu W. Investigations on biomass slagging in utility boiler: Criterion numbers and slagging growth mechanisms. Fuel Process Technol 2014;128:499-508.
[32] Niu Y, Du W, Tan H, Xu W, Liu Y, Xiong Y, et al. Further study on biomass ash characteristics at elevated ashing temperatures: The evolution of K, Cl, S and the ash fusion characteristics. Bioresour Technol 2013;129:642-5.
[33] Wang G, Pinto T, Costa M. Investigation on ash deposit formation during the co-firing of coal with agricultural residues in a large-scale laboratory furnace. Fuel 2014;117, Part A:269-77.
[34] Lu G, Yan Y, Cornwell S, Whitehouse M, Riley G. Impact of co-firing coal and biomass on flame characteristics and stability. Fuel 2008;87:1133-40.
[35] Smart JP, O'Nions P, Riley GS. Radiation and convective heat transfer, and burnout in oxy-coal combustion. Fuel 2010;89:2468-76.
[36] Grimm A. Experimental studies of ash transformation processes in combustion of phosphorus-rich biomass fuels [dissertation]. Luleå University of Technology; 2012.
[37] Lindström E, Sandström M, Boström D, Öhman M. Slagging characteristics during combustion of cereal grains rich in phosphorus. Energy Fuels 2007;21:710-7.
[38] Baptiste F. Numerical and experimental characterization of drop tube furnace and ash deposition analysis [dissertation]. RWTH Aachen University; 2013.

[39] Badzioch S, Hawksley PGW. Kinetics of thermal decomposition of pulverized coal particles. Ind Eng Chem Process Des Dev 1970;9:521-30.
[40] Ma L, Gharebaghi M, Porter R, Pourkashanian M, Jones JM, Williams A. Modelling methods for co-fired pulverised fuel furnaces. Fuel 2009;88:2448-54.
[41] Magnussen BF, Hjertager BH. On mathematical modeling of turbulent combustion with special emphasis on soot formation and combustion. Proc Combust Inst 1977;16:719-29.
[42] Backreedy RI, Fletcher LM, Ma L, Pourkashanian M, Williams A. Modelling pulverised coal combustion using a detailed coal combustion model. Combust Sci Technol 2006;178:763-87.
[43] Ma L, Jones JM, Pourkashanian M, Williams A. Modelling the combustion of pulverized biomass in an industrial combustion test furnace. Fuel 2007;86:1959-65.
[44] Chen L, Ghoniem AF. Development of a three-dimensional computational slag flow model for coal combustion and gasification. Fuel 2013;113:357-66.
[45] Chen HC, Patel VC. Near-wall turbulence models for complex flows including separation. AIAA J 1988;26:641-8.
[46] Kader BA. Temperature and concentration profiles in fully turbulent boundary layers. Int J Heat Mass Tran 1981;24:1541-4.
[47] Baxter LL. Ash deposit formation and deposit properties. A comprehensive summary of research conducted at Sandia's combustion research facility [Technical Report]. Sandia National Labs; 2000 Aug.
[48] Barker B, Casaday B, Shankara P, Ameri A, Bons J. Coal ash deposition on nozzle guide vanes—Part II: computational modeling. J Turbomach 2013;135:011015.
[49] Bouhairie S, Chu VH. Two-dimensional simulation of unsteady heat transfer from a circular cylinder in crossflow. J Fluid Mech 2007;570:177-215.
[50] Nutalapati D, Gupta R, Moghtaderi B, Wall TF. Assessing slagging and fouling during biomass combustion: A thermodynamic approach allowing for alkali/ash reactions. Fuel Process Technol 2007;88:1044-52.
[51] Bale CW, Bélisle E, Chartrand P, Decterov SA, Eriksson G, Hack K, et al. FactSage thermochemical software and databases — recent developments. Calphad 2009;33:295-311.
[52] Fryda L, Sobrino C, Cieplik M, van de Kamp WL. Study on ash deposition under oxyfuel combustion of coal/biomass blends. Fuel 2010;89:1889-902.
[53] Tortosa Masiá AA, Buhre BJP, Gupta RP, Wall TF. Characterising ash of biomass and waste. Fuel Process Technol 2007;88:1071-81.
[54] Aho M, Ferrer E. Importance of coal ash composition in protecting the boiler against chlorine deposition during combustion of chlorine-rich biomass. Fuel 2005;84:201-12.
[55] Tortosa Masiá A. Characterisation and prediction of deposits in biomass co-combustion [dissertation]. Delft University of Technology; 2010.
[56] Plaza P, Griffiths AJ, Syred N, Rees-Gralton T. Use of a predictive model for the impact of cofiring coal/biomass blends on slagging and fouling propensity. Energy Fuels 2009;23:3437-45.
[57] Yakaboylu O, Harinck J, Gerton Smit KG, de Jong W. Supercritical water gasification of manure: A thermodynamic equilibrium modeling approach. Biomass Bioenerg 2013;59:253-63.
[58] Zhang L, Ninomiya Y. Transformation of phosphorus during combustion of coal and sewage sludge and its contributions to PM10. Proc Combust Inst 2007;31:2847-54.
[59] Mao T, Kuhn DCS, Tran H. Spread and rebound of liquid droplets upon impact on flat surfaces. AIChE J 1997;43:2169-79.
[60] Ansys, 15.0 Theory Guide, 2013.
[61] Zhang Z, Kleinstreuer C, Hyun S. Size-change and deposition of conventional and composite cigarette smoke particles during inhalation in a subject-specific airway model. J Aerosol Sci 2012;46:34-52.
[62] Wigley F, Williamson J, Riley G. The effect of mineral additions on coal ash deposition. Fuel Process Technol 2007;88:1010-6.

Table 1. Coal and PKE properties used in the calculations [24, 34, 35].

Ash composition (wt.%)			Proximate analysis (wt.%)(ar)		
	SAC	PKE		SAC	PKE
SiO_2	54.1	15.1	Volatiles	26.4	71.6
Al_2O_3	33.5	3.2	Fixed carbon	60.2	28.4
Fe_2O_3	3.1	5.3	Ash	12.1	4.2
CaO	4.1	10.7	GCV(MJ/kg)	27.3	18.7
MgO	1.3	12.0	Ultimate analysis (wt.%)(daf)		
K_2O	0.7	9.7	C	70.0	44.2
Na_2O	0.1	0.3	H	3.9	7.0
TiO_2	1.7	0.1	O	7.3	46.2
MnO	0.0	1.0	N	1.7	2.6
P_2O_5	1.1	42.7	S	0.6	0.5

Table 2. Chemical fractionation (percentage) of ash components leached from fuels [53, 54].

	SiO_2	Al_2O_3	Fe_2O_3	CaO	MgO	K_2O	Na_2O	TiO_2	P_2O_5
SAC	0	0	0	70	0	2	40	0	0
PKE	1	0	0	5	3	100	100	0	3

Figure Captions

Figure 1. A schematic diagram of the geometry of the EFR based [23, 24].

Figure 2. Schematic diagram of the main formation of the different deposition layers on the front surface of the cylindrical probe.

Figure 3. The methodology for the revised particle impaction model.

Figure 4. The flow configuration and boundary conditions of the 2D computational domain.

Figure 5. The impaction correction factor and comparisons of the predicted particle impaction efficiency using a coarse mesh and the DNS, with and without particle impact correction when (a): Re_t=100 and (b): Re_t=1685 as a function of the Stokes number.

Figure 6. The arrival rate of fly ash particles that impact the probe surface as a function of the number of cells and the impaction efficiency of particles as a function of the particle Stokes number for 0.7M and 1.6M.

Figure 7. The impaction correction factor and impaction efficiency of particles as a function of the particle Stokes number.

Figure 8. The overall impaction efficiency for SAC and for different levels of PKE with and without the revised particle impaction model.

Figure 9. The overall sticking efficiency for SAC and for different levels of PKE.

Figure 10. A comparison between the computed and the experimental data of the deposition efficiency for the SAC with different levels of PKE.

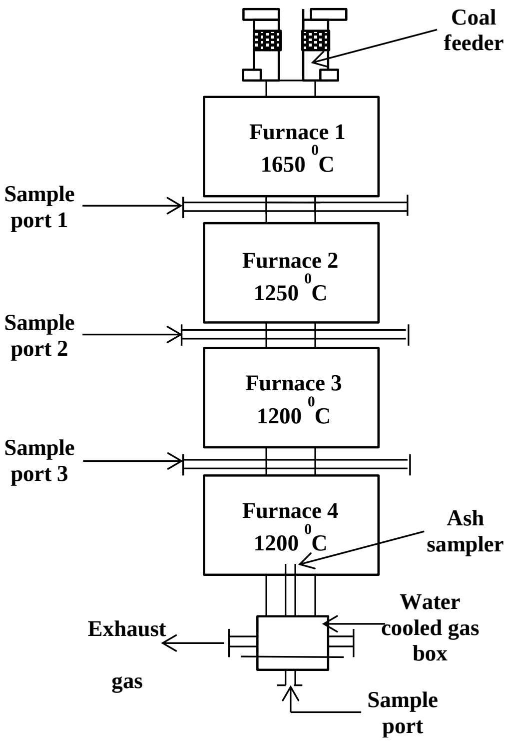

Figure 1. A schematic diagram of the geometry of the EFR based [23, 24].

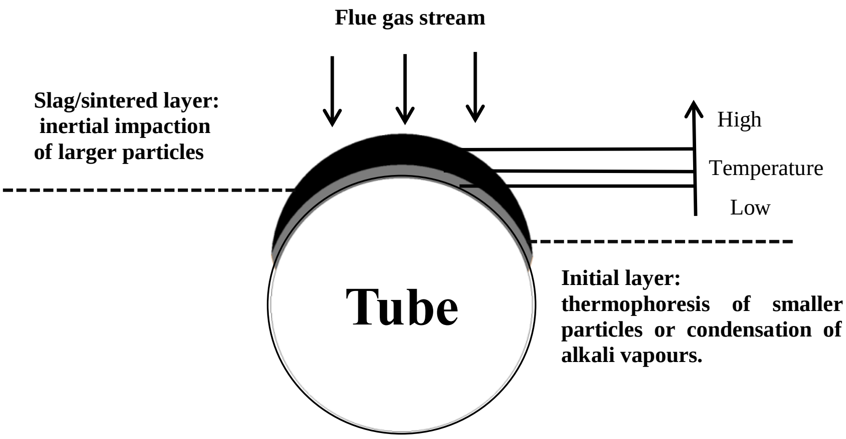

Figure 2. Schematic diagram of the main formation of the different deposition layers on the front surface of the cylindrical probe.

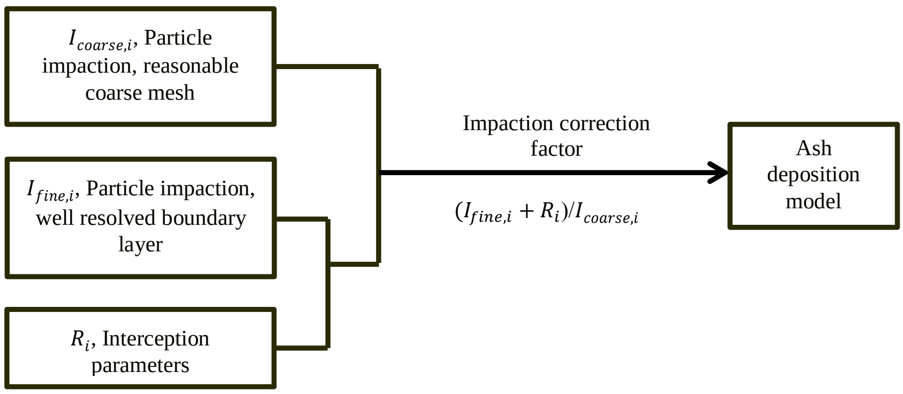

Figure 3. The methodology for the revised particle impaction model.

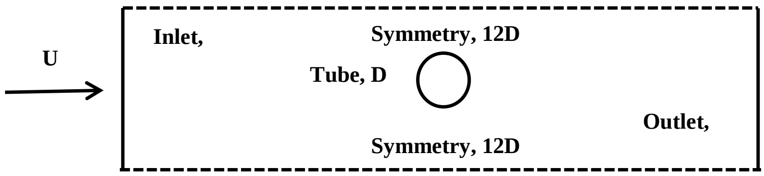

Figure 4. The flow configuration and boundary conditions of the 2D computational domain.

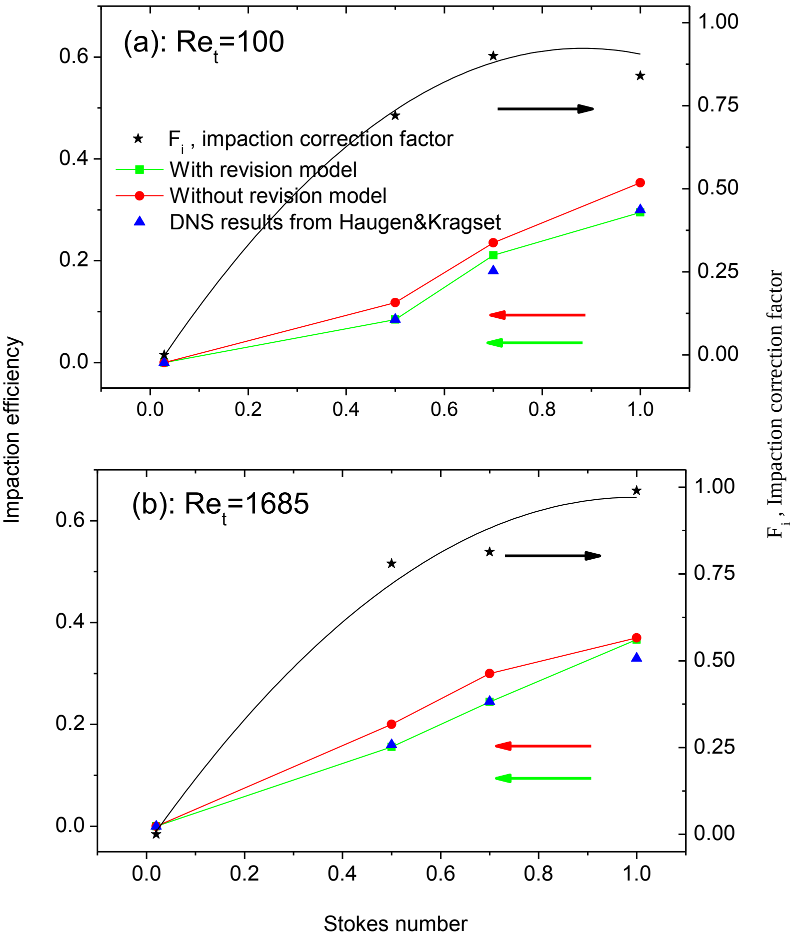

Figure 5. The impaction correction factor and comparisons of the predicted particle impaction efficiency using a coarse mesh and the DNS, with and without particle impact correction when (a): Re_t=100 and (b): Re_t=1685 as a function of the Stokes number.

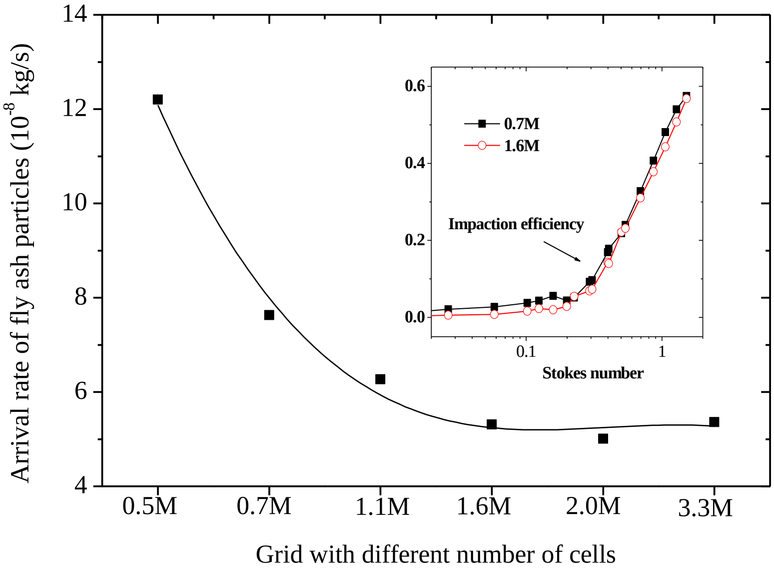

Figure 6. The arrival rate of fly ash particles that impact the probe surface as a function of the number of cells and the impaction efficiency of particles as a function of the particle Stokes number for 0.7M and 1.6M.

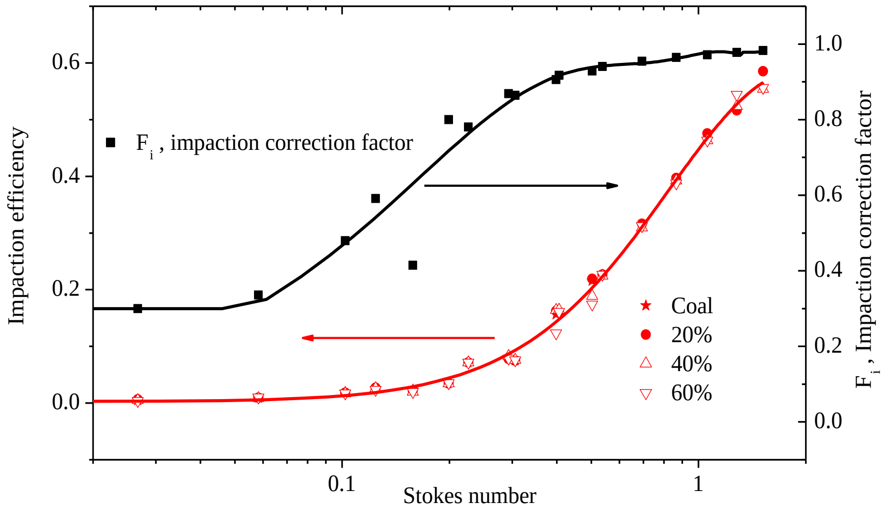

Figure 7. The impaction correction factor and impaction efficiency of particles as a function of the particle Stokes number.

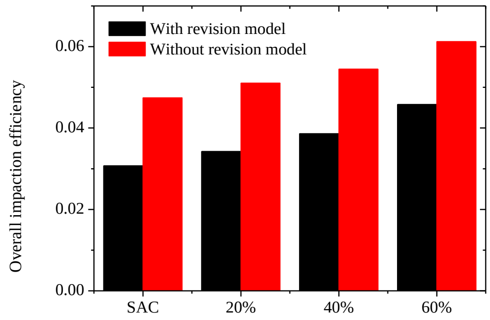

Figure 8. The overall impaction efficiency for SAC and for different levels of PKE with and without the revised particle impaction model.

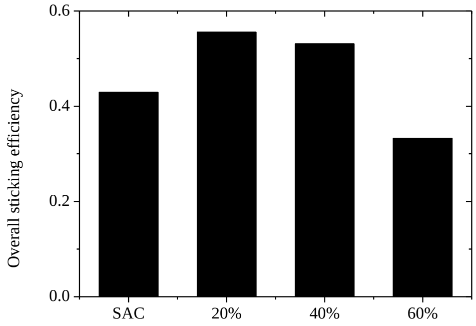

Figure 9. The overall sticking efficiency for SAC and for different levels of PKE.

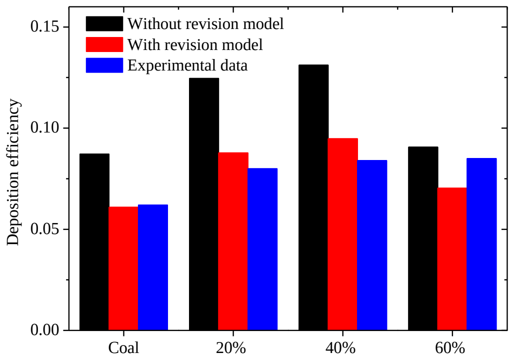

Figure 10. A comparison between the computed and the experimental data of the deposition efficiency for the SAC with different levels of PKE.